PAPER

On the photoevaporation, dust polarization and kinematics of two nebulae in Sh2-236

RAA 2021 Vol. **21** No. **4**, 87(11pp) doi: 10.1088/1674-4527/21/4/87

http://www.raa-journal.org *http://iopscience.iop.org/raa*

***R**esearch in*
***A**stronomy and*
***A**strophysics*

On the photoevaporation, dust polarization and kinematics of two nebulae in Sh2-236

Archana Soam

SOFIA Science Center, Universities Space Research Association, NASA Ames Research Center, M.S. N232-12, Moffett Field, CA 94035, USA; *asoam@usra.edu*
Korea Astronomy and Space Science Institute, 776 Daedeokdae-ro, Yuseong-gu, Daejeon, Republic of Korea

Received 2020 July 23; accepted 2020 October 8

Abstract In the work presented here, the impact of magnetic field on the dynamical evolution of cometary globules Sim 129 and Sim 130 in the Sh2-236 H II region and the ionized gas streaming out of their surfaces is investigated. The magnetic field morphology in the region associated with these globules is inferred using optical polarization measurements with the Sampurnanand Telescope at ARIES. The nebular emission is probed through radio continuum mapping at 1.4 GHz with the archival National Radio Astronomy Observatory (NRAO) Very Large Array (VLA) Sky Survey (NVSS) data. The correlation of these measurements suggests that photoevaporated gas from the surfaces of Sim 129 and Sim 130 accumulates in clouds and starts streaming along the magnetic field lines. The ^{12}CO (J=1–0) molecular line observations are performed towards NGC 1893 from the 14-m single dish radio telescope in Taeduk Radio Astronomy Observatory (TRAO). The velocity dispersion in the ^{12}CO (J=1–0) molecular line and the dispersion in polarization angles are considered in the Davis-Chandrasekhar-Fermi formulation to estimate the magnetic field strength towards two Sim nebulae. The average value of field strength is found to be $\sim$60 μG with uncertainty of 0.5 times the estimated value.

Key words: ISM: general — polarization: nebulae

1 INTRODUCTION

In the presence of a magnetic field, the dynamical evolution of the globules and ionized gas streaming out of their surfaces get modified significantly depending on the strength of the magnetic field and its orientation with respect to incoming ionizing photons (Henney et al. 2009). This is understandable because, in the ideal magnetohydrodynamics (MHD) limit, matter is well coupled to the magnetic field lines and when the field is sufficiently strong, the magnetic pressure and tension strongly resist any movement of gas in the direction perpendicular to the field orientations. However, no such resistance is offered for the gas motion along the field lines because ionized species can easily move along fields lines. Henney et al. (2009) presented the first three-dimensional (3-D) MHD simulations towards magnetized globules and found that photoevaporating globules will evolve into more flattened sheet like structures compared to the non-magnetic cases when the cloud initially has a strong B-field (i.e. 100 times the thermal pressure) perpendicular to the ultraviolet (UV) radiation direction. The photoevaporated gas accumulates between the ionizing source and the cloud making a recombination region which further prevents the supply of ionizing flux from reaching the globule from the ionizing source. Studies have attempted to explain this scenario through MHD simulations (Mackey & Lim 2011). These simulations can be tested by tracing the magnetic field orientation with respect to the ionizing radiation in the nebulae sitting on the periphery of H II regions (Soam et al. 2018). Assuming the gas is totally ionized, the total pressure of the ionized layer on the surface of the globule with respect to the internal neutral gas can be estimated.

These parameters hold the potential to provide useful insight into the dynamical states of globules in H II regions and enable us to understand the radiation driven implosion (RDI) process. RDI is a process in which radiation from massive stars drives an implosion into the globules sitting in the vicinity. This process drives the convergent shock into the globule and causes it to implode due to compression. Using molecular line measurements in the periphery of H II regions, we can investigate the kinematics of gas in those regions. Polarization and radio spectroscopic observations together provide the

opportunity to investigate magnetic field structure and associated gas kinematics.

In this work, I studied two nebulae, Sim 129 and Sim 130, in the vicinity of a young open cluster NGC 1893 located at the center of H II region Sh2-236 (a.k.a. IC 410). This region is populated by several massive O and B type stars (Maheswar et al. 2007). A detailed list of the high mass stars and their type is presented by Maheswar et al. (2007). Among the listed five O type stars, namely HD 242926 (BD+33 1024, LSV +33°16), NGC 1893 HOAG4 (LS +33°15), HD 242935 (BD+33 1026), BD+33 1025 (LSV +33°17, NGC 1893 HOAG5) and HD 242908 (NGC 1893 HOAG5, BD +33 1023), the central O7.5V type star (Negueruela et al. 2007) HD 242935 is found to be a potential candidate responsible for ionizing the surrounding medium.

Here I present the magnetic field geometry of NGC 1893 utilizing optical R-band polarimetry. Near-infrared (NIR) (H-band) polarimetric observations towards this object have also been carried out using SIRPOL (in prep. by Eswaraiah et al). This region displays a smaller angular size (∼10 arcmin) at a distance of 3.2 kpc which makes it easier to cover with only a few pointings. This enables us to cover the whole region by observing a few fields. At the above quoted distance of this cluster, the extent of the two nebulae Sim 129 and Sim 130 is of the order of $\sim$ 4.5 pc (with a diameter of head $\sim$ 1.0 pc) whereas the distance between the nebulae and the ionizing source is $\sim$ 6 pc. The morphology of the nebular emission and its orientation with respect to the magnetic field geometry is probed by relying on the archival National Radio Astronomy Observatory (NRAO) Very Large Array (VLA) Sky Survey (NVSS) data at 1.4 GHz. The estimation of photoionizing flux impinging on the two nebulae and comparison of it with the expected flux from the O-type stars located towards the region have also been performed. This paper is structured as follows. Section 2 elaborates on the observations and data reduction procedures and the results are presented in Section 3. The analysis of the results and a summary of this study are discussed in Sections 4 and 5, respectively.

2 OBSERVATIONS AND DATA REDUCTION

2.1 Optical Polarization Observations Using AIMPOL

Polarimetric observations were carried out with the 104-cm Sampurnanand telescope of Aryabhatta Research Institute of Observational Sciences (ARIES), Nainital, India employing the Aries IMaging POLarimeter (AIMPOL). We used R-band (standard Johnson R_c filter having $\lambda_{R_{\rm eff}}$=0.630 µm) in polarimetric observations of two fields towards NGC 1893. The polarimeter has a half wave plate (HWP) modulator and a Wallaston prism. The data reduction procedure with details on image size, CCD characteristics, pixel size and calculation of Stokes parameters at four different angles of HWP are explained in my earlier work (Soam et al. 2013, 2015). The instrumental polarization has been removed from the observed target stars by observing the unpolarized standards given in Schmidt et al. (1992).

2.2 Molecular Line Observations from TRAO

On-The-Fly (OTF) mapping observations covering a region of $28^{'} \times 28^{'}$ towards NGC 1893 were carried out on 2016 March 4 and 5 for the molecular transitions CO (J=1–0) and $C^{18}O$ (J=1–0) (with $V_{\rm LSR} = -7.0$ km s^{-1}) at Taeduk Radio Astronomical Observatory (TRAO). This is a 13.7 m single dish mm wave telescope equipped with the SEcond QUabbin Observatory Imaging Array (SEQUOIA) at Korea Astronomy & Space Science Institute, South Korea. SEQUOIA has an array of 4×4 pixels and operates in the 85−115 GHz frequency range. The system temperature is generally found to be 250 K (85−110 GHz) to 500 K (115 GHz; ^{12}CO). SEQUOIA provides facilities for simultaneous observations in two different tracers within a frequency band of 15 GHz. The beam size (half power beamwidth, HPBW) and main-beam efficiency in CO is found to be $44^{''}$ and 51%±2% (Liu et al. 2018). I observed the target for $\sim$ 180 minutes to achieve a root mean square (rms) of 0.3 K in the $T_A{}^*$ scale in CO. Observations of an emission free region within the 2° field of the target coordinates were used to subtract the sky signal. The signal-to-noise ratio is estimated to be ∼16 at the brightest position of $T_A{}^*$ $\sim$ 4.8 K. The achieved velocity resolution is $\sim$ 0.25 km s^{-1}. An SiO maser was utilized for pointing and focusing the telescope. The pointing of the telescope was as good as $\sim$ $5-7^{''}$. Data reduction was performed using CLASS from GILDAS[1].

3 RESULTS

3.1 Optical Polarimetric Results

The results of optical polarization for 123 sources observed (combining our measurements and previous polarimetric results reported by Eswaraiah et al. 2011) towards NGC 1893 are discussed. Eswaraiah et al. (2011) observed 44 stars in V-band. Our polarization angles are consistent with those of their results. The nebula Sim 130 was not covered in the previous polarization observations by Eswaraiah et al. (2011). In this work, I covered the two nebulae by imaging deeper into the cloud and increased the sample to get a relatively high spatial resolution magnetic field geometry in the region between HD 242935 and the two nebulae. The range of degree of polarization (P) is from 0.5% to 6.0%. The mean values of P and polarization

[1] Grenoble Image and Line Data Analysis Software; https://www.iram.fr/IRAMFR/GILDAS/

position angle (θ_P) with corresponding standard deviation are 2.7%±1.0% and 179° ± 11°, respectively. I have chosen only those measurements for which the ratio of P and the error in P (σ_P), P/σ_P, is ≥ 2 (this criterion provides the statistically significant number of data points). The observed polarization vectors are plotted on the WISE 12 μm image of NGC 1893, displayed in the left panel of Figure 1. The distribution of position angles with polarization fraction is plotted in the right panel of the figure. Figure 2 shows the variation in amount of polarization and position with distances of the targets in the left and right panels, respectively.

Figure 3 features the color composite image (constructed using WISE bands 1, 2 and 4) of H II region IC 410 containing NGC 1893. The dusty structure of this H II region is clearly seen in this figure. The expanding surrounding medium is clearly depicted in the image. The figure is labeled with positions of ionizing source HD 242935 and other O type stars, and the nebulae Sim 129 and 130. The mean magnetic field directions in the nebulae are marked with cyan color line segments. The image affirms that the inherent magnetic fields in the region were mostly parallel to the GP. The shape of nebulae suggests that their surface material is mostly photoevaporated by the ionizing radiation from a central O type star, leaving behind the smoky, thin shaped and elongated cloud structure (Zealey et al. 1983; Sugitani et al. 1991).

3.2 Archival Radio Data

The NVSS 1.4 GHz image of the region in IC 410 is featured in Figure 4. The radio 1.4 GHz is overplotted on the WISE 12 μm image. The NVSS map does not give much information due to its poor resolution and sensitivity but still the wall of the H II region and location of two nebulae Sim 129 and 130 are clearly visible. The resolution of this map is $45''$ at 1.4 GHz. The radio fluxes at nebulae Sim 129 and 130 are used to estimate some parameters discussed in Section 4.3.

3.3 Estimation of Line Width from CO Molecular Line Observations

Figure 5 displays the CO contours overplotted on the WISE 12 μm image containing the IC 410 region. I found three components of the CO line with different $V_{\rm LSR}$, -7.0 km s^{-1}, -2.5 km s^{-1} and 2.5 km s^{-1}, associated with this cloud which are shown using white, cyan and green color contours, respectively in Figure 5. The red line segments are normalized polarization vectors (where lengths of the vectors do not depend on polarization fraction) plotted to infer the magnetic field morphology in the region. I considered all the three components of CO emission since they coincide with locations of the cloud region where I carried out optical polarimetric observations. The insets in Figure 5 show the average spectra of the CO emission. The width of the spectral line is generally expressed in terms of full width at half-maximum (FWHM) when the line profile is represented well by a Gaussian shape. From the OTF map in the CO (J=1–0) molecular line towards NGC 1893, I estimated the CO line width as it traces the low density region where optical polarization observations cover the cloud. The CO line width of the average spectra of the component with $V_{\rm LSR}$ -7.0 km s^{-1} is found to be 2.27±0.03 km s^{-1} and that of the other two components with $V_{\rm LSR}$ -2.5 km s^{-1} and $V_{\rm LSR}$ 2.5 km s^{-1} are found to be 1.95±0.04 km s^{-1} and 2.9±0.09 km s^{-1}, respectively. The average value of FWHM in these components is identified to be 2.37±0.10 km s^{-1}. I measure CO line widths by fitting Gaussian profiles to the line spectra.

4 DISCUSSION

4.1 Distance and Interstellar Polarization Subtraction

Since NGC 1893 is located at a distance of 3.2 kpc (Sharma et al. 2007), our polarimetric results towards NGC 1893 may have some contamination introduced by interstellar medium (ISM) polarization in the line of sight. Therefore it is necessary to remove the foreground polarization contribution from our results. Eswaraiah et al. (2011) presented multiband optical polarization observations of this region. They observed clusters located between 600 pc (NGC 2281) and 3.2 kpc (NGC 1893) including NGC 2281, NGC 1960 and Stock 8, along with NGC 1664, to investigate the dust properties towards the Galactic anticenter. They reported two dust layers at distances of ∼170 pc and ∼360 pc based on distributions of P_V and θ_V (polarization observations in V band). The first dust layer is found to have P_V ∼0.3%–0.9% and θ_V ∼20°–50° and the second layer is found to have P_V $\sim$ 1.0% − 1.9% and θ_V $\sim$ 110°–150°. The maximum amount of polarization produced by the two layers is found to be $P_V \sim 2.2\%$.

In order to remove the foreground interstellar polarization from our results, I used the polarization values of the cluster Stock 8 with Galactic coordinates of $\ell = 173.37°$ and $b = -0.18°$. The Galactic coordinates of NGC 1893 are $\ell = 173.59°$ and $b = -1.68°$. Since Stock 8 is at a distance of 2.5 kpc (Jose et al. 2008), I assumed that it carries the maximum contribution of all the material present in the foreground of NGC 1893. I estimated the mean values of P and θ_P towards this cluster. I then estimated the Stokes parameters $q(= P\cos 2\theta)$ and $u(= P\sin 2\theta)$ considering the polarization values towards Stock 8. I calculated the mean values of these Stokes parameters and named them $Q_{\rm fg}$ and $U_{\rm fg}$ respectively. The

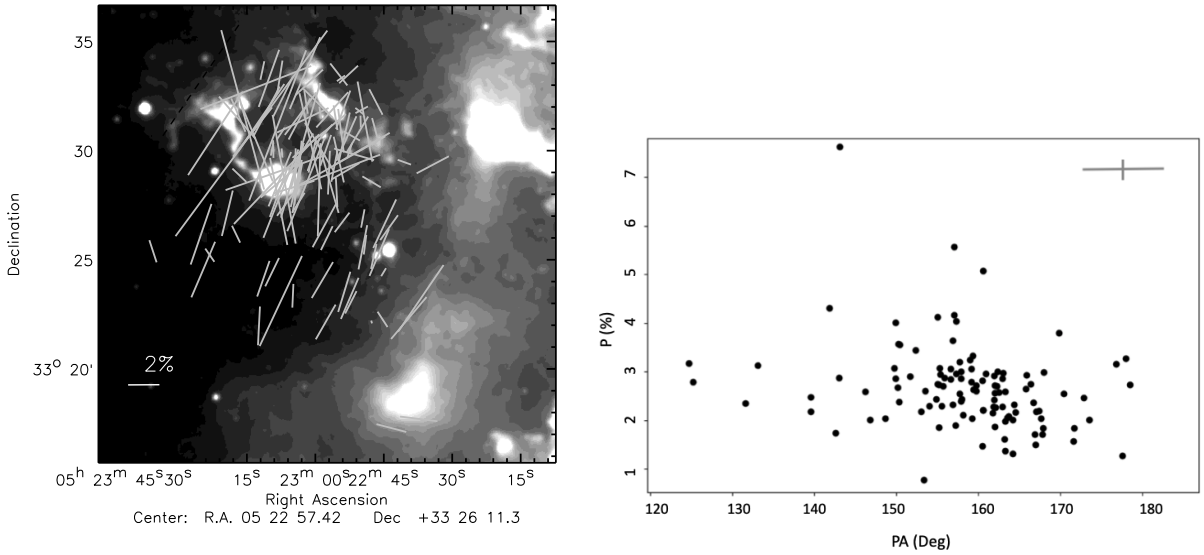

Fig. 1 *Left panel*: The polarization vectors plotted after correcting for the interstellar polarization. *Right panel*: The P vs. θ_P distribution of measurements. A symbol signifying typical errors in P and θ_P values is also marked.

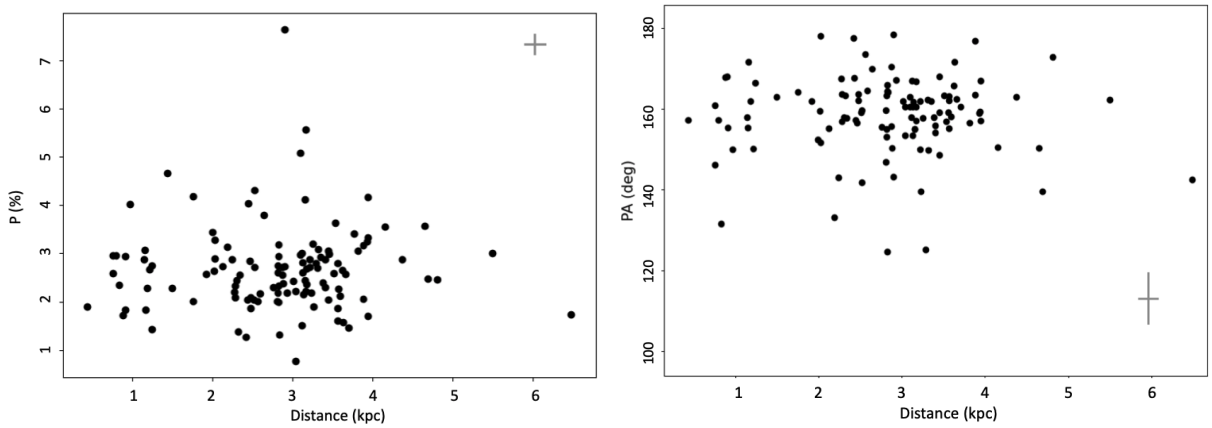

Fig. 2 *Left* and *right* panels depict variations of P and PA with distances (Gaia Data Release 2 (DR2); Bailer-Jones et al. 2018) of the stars respectively.

mean values of foreground Stokes parameters $Q_{\rm fg}$ and $U_{\rm fg}$ are estimated to be 1.458 and –1.139, respectively. Then I calculated the Stokes parameters, $Q_\star$ and $U_\star$, of the target sources. The Stokes parameters Q_c and U_c representing the foreground corrected polarization of the target stars are calculated by applying the expression

$$Q_c = Q_\star - Q_{\rm fg}, U_c = U_\star - U_{\rm fg}\,. \quad (1)$$

The corresponding foreground corrected degree of polarization P_c and position angle θ_c of the target stars are calculated by relying on the equations

$$P_c = \sqrt{(Q_c)^2 + (U_c)^2}, \theta_c = 0.5 \times \tan^{-1}\left(\frac{U_c}{Q_c}\right)\,. \quad (2)$$

The histograms of uncorrected and foreground corrected polarization position angles are drawn in Figure 6. Both populations have two components centered around values of 10° and 150°. This suggests that these components are inherent in the cloud. The corrected polarization vectors are overlaid on the WISE 12 μm image of NGC 1893 shown in the left panel of Figure 1.

4.2 Ricean Bias Correction in Polarization

After removal of foreground contributions, I corrected the polarization values for Ricean bias following the approach mentioned in Sohn (2011). Ricean bias occurs in linear polarization measurements. Sohn (2011) reviewed two methods for this correction. One method was developed by Wardle & Kronberg (1974) and the other similar method was developed by Killeen et al. (1986). In the first method, a good approximate solution for Ricean bias correction is given by $I_p \sim \sqrt{{I_{p_{\rm obs}}}^2 - \sigma^2_{I_{p_{\rm obs}}}}$. Here, I_p, $I_{p_{\rm obs}}$ and $\sigma_{p_{\rm obs}}$

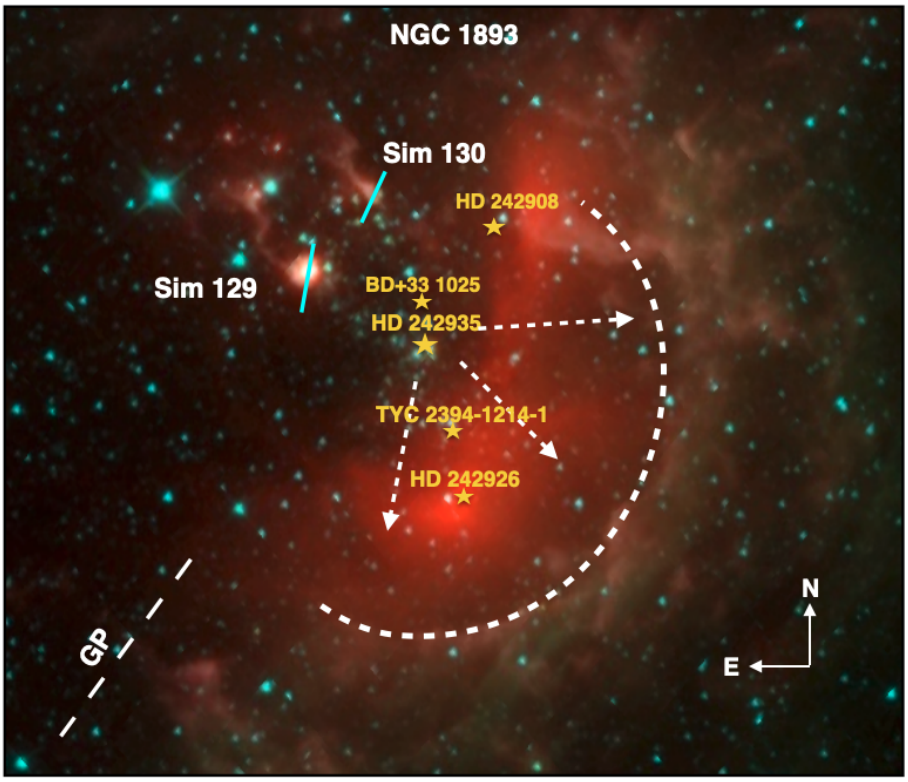

Fig. 3 Figure features the color composite (RGB) image of H II region IC 410 made utilizing WISE 1 (3.4 μm), 2 (4.6 μm), and 4 (12 μm) band data containing open cluster NGC 1893. The image is labeled with the positions of nebulae Sim 129 and Sim 130. Locations of five O type stars including HD 24293 are also marked in the image. The cyan line segments plotted on the nebulae represent the mean magnetic field orientation in these regions. The expanding region created by ionizing radiation from HD 242935 is signified by a dashed circle. The position of the Galactic plane (GP) is traced with a white dashed line and the north and east directions are also presented.

are bias corrected polarized intensity, observed value of polarized intensity and associated uncertainties in $I_{p_{\rm obs}}$, respectively. The other solution for Ricean bias correction given by Killeen et al. (1986) assumes the above relation as $I_p \sim I_{p_{\rm obs}} - 0.5{\sigma_{p_{\rm obs}}}^2/I_{p_{\rm obs}}$. I applied both these methods explained in Sohn (2011) to perform the Ricean correction to polarization values. The Gaussian fitted histograms of uncorrected and corrected values using two methods are shown in Figure 7. The difference in the corrected and uncorrected values is not huge and both methods deliver quite similar values.

4.3 Magnetic Field Geometry and Strength

The field geometry in NGC 1893 becomes complex after subtracting the foreground polarization component. Figure 8 features the normalized polarization vectors (i.e. length of the line segment is independent of the fraction of polarization) corresponding to the higher signal-to-noise ratio (with $P/\sigma_P > 2.5$) data overlaid with 1.4 GHz continuum contours on the WISE 12 μm image of the NGC 1893 region. Towards nebula Sim 129, it is apparent that the field lines are curved in the outward direction which is opposite to the morphology normally seen in some cometary globules (CGs) such as LBN 437 (Soam et al. 2013). Such field geometry has been seen in the CG 30–31 complex by Targon et al. (2011). This might be caused by gas streaming off from the head part of Sim 129 due to the presence of ionizing radiation from O type stars including HD 242935. This cloud is relatively closer to the ionizing radiation as compared to nebula Sim 130. Therefore, the effect of UV photons is relatively higher towards this nebula. The field lines may possibly be following the ionized gas photoevaporating in the outward direction assuming that matter is coupled to the field lines. This will make the field lines curve towards the outward direction. A bimodal distribution of the position angles towards NGC 1893 can be noticed in Figure 9. The direction of ionizing photons is signified with green arrows in Figure 8. This direction of radiation is in the plane of the sky and is simply obtained by visual estimation. The radiation is impinging on the head of Sim 129 at $\sim 60^\circ$ and the mean direction of magnetic fields in the cloud is 155° (see Fig. 8). The offset of 95° between the ionizing radiation and the magnetic fields suggests that the magnetic field lines are perpendicular to the incoming UV radiation. Such results can be compared to the 3-

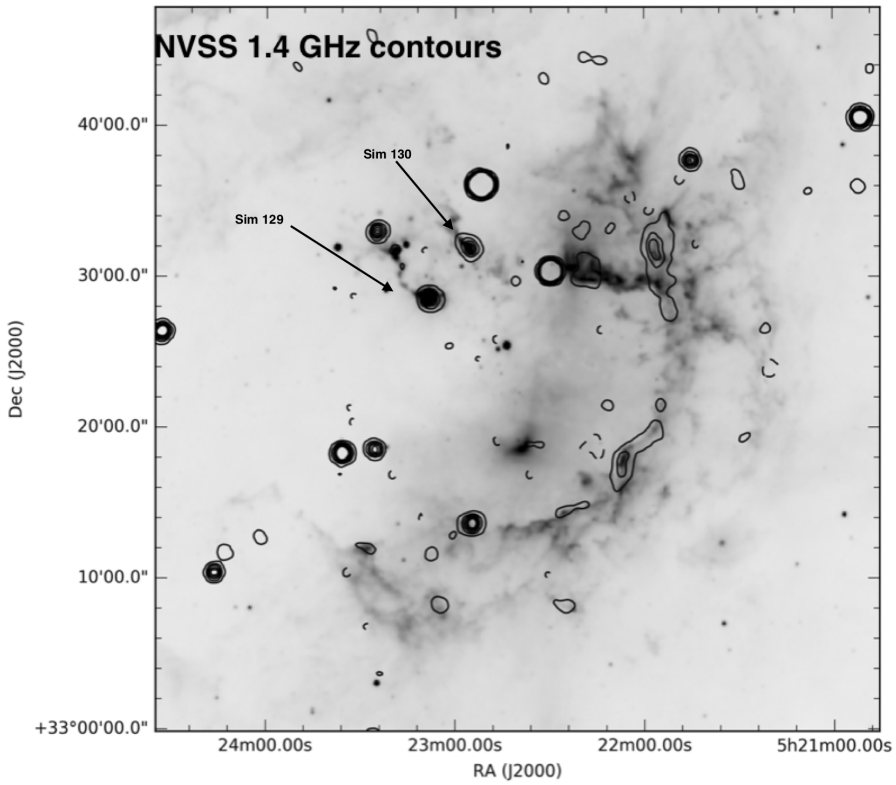

Fig. 4 The NVSS 1.4 GHz contours drawn on the WISE 12 μm image of NGC 1893 containing Sim 129 and Sim 130 nebulae.

D MHD simulations presented by Henney et al. (2009). These simulations suggest that the strong perpendicular magnetic fields resist any movement of gas in directions perpendicular to the original field direction, whereas no such magnetic support exists to oppose gas motions along the field lines. As a result, the implosion of the globule by the ionization-driven shock front is highly anisotropic. In the case of weak magnetic fields perpendicular to the ionizing radiation direction, the flattening of the globule along the field lines is much less. In addition, no current sheet forms at the symmetry plane, and the photoevaporation flow is powerful enough to drive all ambient material. By comparing our observations towards the nebula Sim 129 with the simulation, I found that the magnetic fields are relatively weaker and following the material in the streams of ionized gas from the head of the nebula.

Whereas in Sim 130, the magnetic field geometry suggests that the field lines are curved on the cloud head. It seems that the field lines are dragged by the ionizing radiation but in the opposite direction from that seen in Sim 129. This is similar to the field morphology visible in LBN 437 (Soam et al. 2013). The different field morphology in Sim 130 may be because its distance from the ionizing source is relatively larger (projected distances of Sim 129 and Sim 130 from HD 242935 are 3.7 pc and 4.4 pc, respectively at a distance of 3.2 kpc from NGC 1893) than that of Sim 129. The flux reaching this cloud should be relatively lesser because of the condensation of ionized gas between the source HD 242935 and the nebula. Therefore the amount of ionization and ionizing gas streaming out of the nebula head should be lesser than that from Sim 129. The field morphology of Sim 129 may be more chaotic due to a higher amount of ionizing photons and hence higher pressure compared to the magnetic pressure. This might not be the case in Sim 130. The histogram and distribution of position angle with degree of polarization is also depicted in Figure 9. There is a component of θ_P appearing in Figure 9 peaking at around $\sim 10^{\circ}$. The direction of ionizing radiation impinging on this nebula head is also $\sim 10^{\circ}$. This suggests that the field lines become almost parallel to the ionizing radiation in Sim 130. MHD simulations towards such morphology of magnetic field are presented by Williams et al. (2001) showing the curved field lines on the head of the cloud. The field lines may be dragged by incoming ionizing radiation. There is a visible component of θ_P appearing at $\sim 150^{\circ}$ in both the nebulae but it is more prominent in Sim 129. This component is almost perpendicular to the average direction of ionizing radiation in the plane of the sky.

I tried to investigate the structural evolution of nebulae Sim 129 and 130 in the context of magnetic fields by

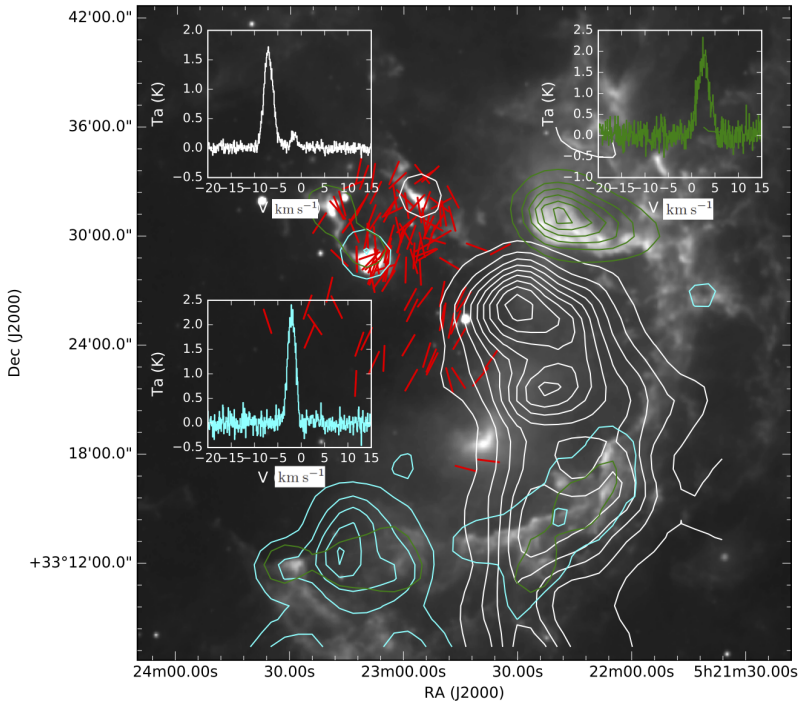

Fig. 5 WISE 12 μm image of NGC 1893 with overplotted CO (J=1–0) integrated intensity contours corresponding to three velocity components with $V_{\rm LSR}$ -7.0 km s^{-1} (*white*), –2.5 km s^{-1} (*cyan*) and $V_{\rm LSR}$ 2.5 km s^{-1} (*green*) in the line of sight. The average spectra corresponding to these emissions are featured in the insets. The x axes of the insets represent the velocity and the y axes signify the antenna temperature. The red segments are normalized polarization vectors (independent of polarization fraction) illustrating the magnetic field morphology in this region.

drawing a diagram in Figure 10. The left panel in this figure shows the initial geometry of magnetic fields in the region and the location of two possibly preexisting clouds on the periphery of the H II region created by central O type stars including HD 242935 (see Fig. 3). The ionizing radiation photoevaporates the surface material of the two clouds causing more elongated tadpole like structures stretching radially away from the direction of radiation. The modified structures in the nebulae are featured in the right panel of Figure 10. The magnetic fields are modified on the tips of the nebulae based on their distances from the ionizing sources. The modified and curved field lines are also traced by dashed curves in the right panel.

I estimated the plane of the sky ($\rm B_{POS}$) magnetic field strength in the region around Sim 129 and Sim 130 nebulae using the updated Davis-Chandrasekhar-Fermi (DCF) relation ($B_{\rm POS} = 9.3\sqrt{n(H_2)}\delta v/\delta\theta$; Davis 1951; Chandrasekhar & Fermi 1953). Here $n(H_2)$ represents the volume density of the clouds which is taken to be $\sim 10^3\,{\rm cm}^{-3}$, δv is the velocity dispersion and $\delta\theta$ is the dispersion in θ_P, corrected by the uncertainty in θ_P[2] (see details in Lai et al. 2001; Franco et al. 2010). The average value of dispersion in position angles in both the components seen in Figure 9 is measured to be $\sim$ 13°. I measured the ^{12}CO (J=1–0) line width (Δv = 2.3 km s^{-1}) from our observations towards NGC 1893 using TRAO. The corrected dispersion in position angle ($\delta\theta$) is estimated by following the procedure given by Lai et al. (2001) and Franco et al. (2010) utilizing the standard deviation obtained from a Gaussian fit to the θ_P. Applying these values in the DCF relation, I obtained a field strength of $\sim$ 60 μG around the two nebulae with a typical uncertainty ($\sigma B_{\rm POS}$) of $\sim 0.5 B_{\rm POS}$ (Crutcher 2005).

4.4 Pressure Comparison in Sim Nebulae

When a cloud is exposed to high energy radiation from O and B stars, the surface of the cloud get ionized by the incident flux. This ionized gas streams away from the cloud and exerts pressure in the form of a shock front on the cloud. Ionized boundary layer (IBL) pressure can be calculated considering the electron density

[2] The uncertainty in the position angles is calculated by error propagation in the expression of polarization angle θ, which gives $\sigma_\theta = 0.5 \times \sigma_P/P$ in radians, or $\sigma_\theta = 28.65° \times \sigma_P/P$ (see; Serkowski 1974) in degrees.

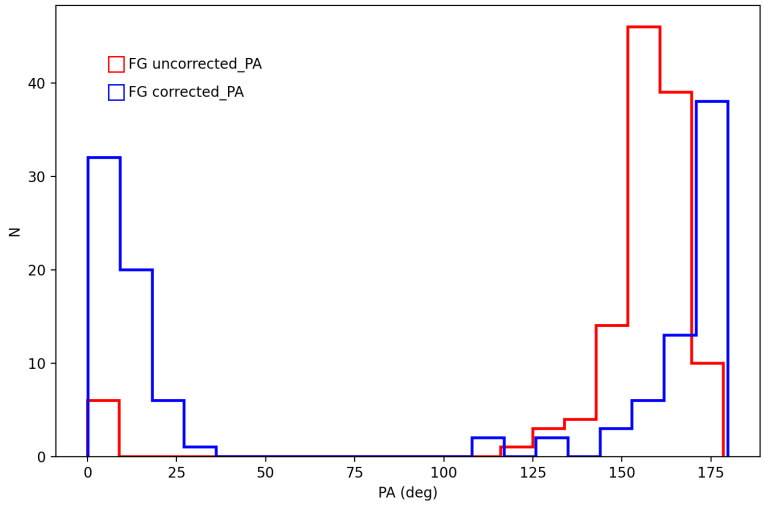

Fig. 6 The histogram of foreground uncorrected and corrected position angles.

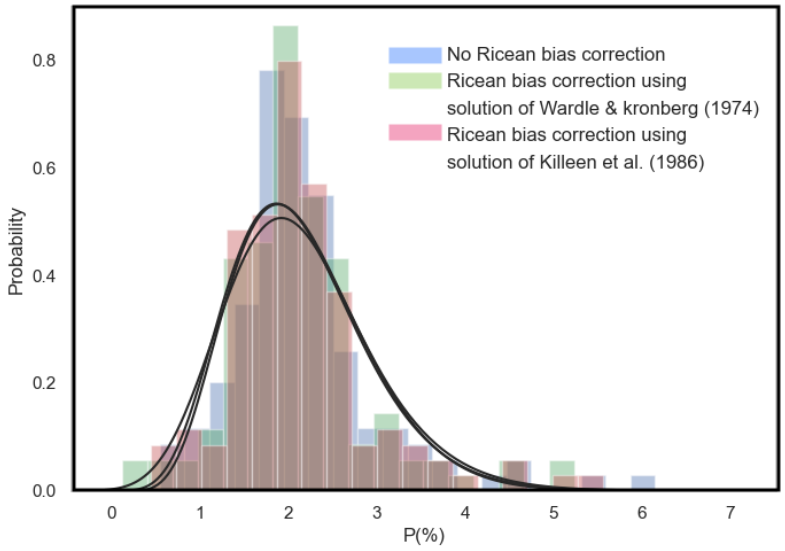

Fig. 7 The histograms of polarization values without and with Ricean bias corrections (Sohn 2011).

estimated with the help of radio flux. It is important to understand the pressure balance in these clouds when we compare the IBL pressure to other pressure terms such as magnetic and internal molecular pressure. I estimated these pressures to investigate the competition between IBL and molecular pressure. This investigation of pressure balance is important to understand because in a pressure equilibrium condition, these clouds are likely to be shocked by photoionization. By using the radio intensities obtained towards the head parts of these nebulae (emission at the centers of the heads of the nebulae in 1.4 GHz), I estimated the flux impinging on the nebula heads. I adopted the method by Morgan et al. (2004) for estimation of the various parameters towards Sim 129 and Sim 130. I calculated the flux (ϕ) reaching the Sim 129 and Sim 130 nebulae using the general equations from Lefloch & Lazareff (1994). They assumed a Gaussian intensity distribution of width θ (HPBW) and derived the relation (provided in eq. 6 of their paper) for a Rayleigh-Jeans brightness flux. Morgan et al. (2004) assume optically thin emission and the region is in photoionization equilibrium. Following a similar approach, I relied on the following relation to estimate the impinging flux,

$$\phi = 1.24 \times 10^{10} S_\nu {T_e}^{0.35} \nu^{0.1} \theta^{-2} \,. \qquad (3)$$

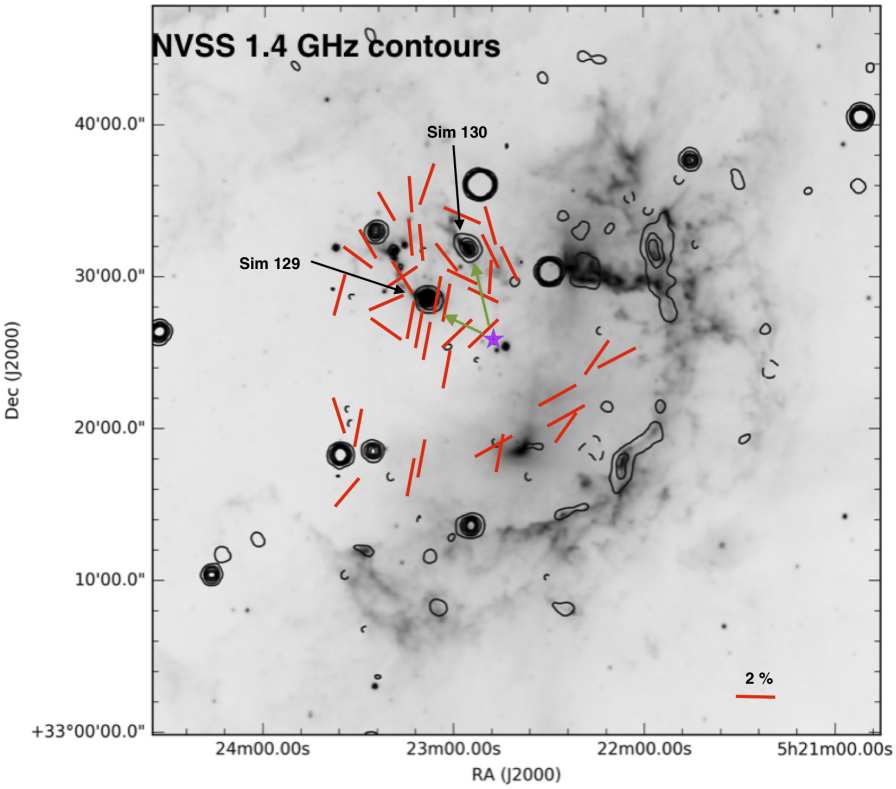

Fig. 8 Same as Fig. 4 with magnetic fields signified using normalized polarization vectors overplotted. The magenta star symbol marks the position of ionizing source HD 242935. The plane of the sky directions for ionizing radiation toward nebulae are illustrated with green vectors.

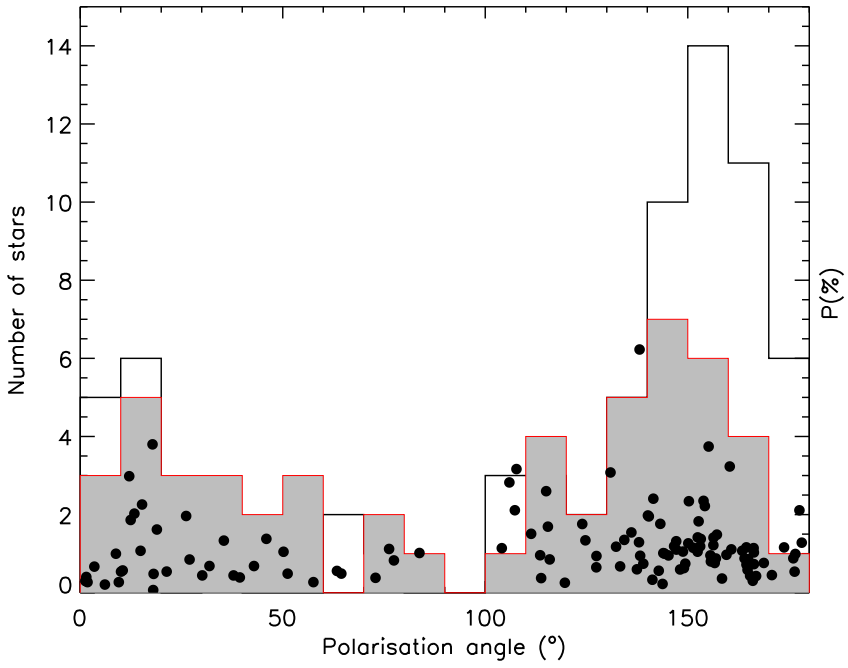

Fig. 9 Histogram of the θ_P values is displayed along with the distributions of P with θ_P. The open histogram corresponds to data from the surroundings of Sim 130 and the filled grey histogram represents the data in the vicinity of Sim 129.

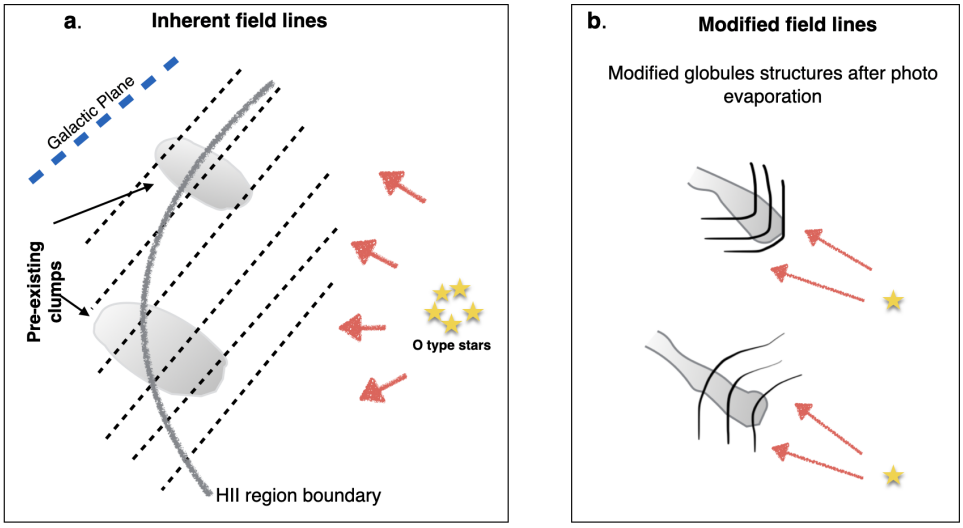

Fig. 10 Figures a and b in the left and right panels illustrate a diagram depicting the initial geometry of field lines with respect to the location of the preexisting nebulae and the modification in the magnetic fields and nebulae structure after being affected by ionizing radiation from central sources, respectively.

Here the symbols S_ν, T_e, ν and θ represent the integrated radio flux in Jy beam^{-1}, effective electron temperature of the ionized gas in K, frequency of the emission in GHz and angular diameter in arcsec over which the emission is integrated. The average values of S_ν over Sim 129 and 130 are found to be 0.021 and 0.024 Jy beam^{-1}, respectively. I used a typical value of electron temperature T_e of 10^4 K. Considering the flux obtained in 1.4 GHz emission from NVSS and an angular diameter of $\sim$ 50 arcsec, I calculated the flux (ϕ) reaching the nebulae. The estimated values of ϕ towards Sim 129 and Sim 130 are found to be 6.2×10^9 cm^{-2} s^{-1} and 5.1×10^9 cm^{-2} s^{-1}, respectively. The subsequent values of electron density estimated towards Sim 129 and Sim 130 are also calculated as

$$n_e = 122.41 \times \sqrt{\frac{S_\nu {T_e}^{0.35} \nu^{0.1} \theta^{-2}}{\eta R}} \qquad (4)$$

where the symbols are the same as expressed in the equation above and η is the effective thickness of the IBL as a fraction of the cloud radius (IBL; typically found to be $\sim$ 0.2 from Bertoldi 1989). R is the radius of the cloud in parsec. The values of electron densities are estimated to be $\sim$250 cm^{-3} and $\sim$230 cm^{-3} towards Sim 129 and Sim 130, respectively. The estimated values of IBL pressure (P_i/k_B; where P_i is the ionizing gas pressure and k_B is the Boltzmann constant) are ascertained to be 25×10^5 cm^{-3} K and 23×10^5 cm^{-3} K in Sim 129 and Sim 130, respectively. These results are comparable to the values reported for some bright-rimmed clouds (BRCs) studied by Thompson et al. (2004). To examine the pressure balance between nebulae, I compared the IBL pressure with internal pressure. For estimating the internal pressure, I relied on our C^{18}O (J=1–0) line observations towards these nebulae using TRAO. I used the turbulent velocity dispersion (σ) of C^{18}O (J=1–0) line and molecular gas density (ρ_m). I applied the relation ($P_m \simeq \sigma^2 \rho_m$) adopted by Morgan et al. (2004) for calculating the molecular pressure in BRCs. The internal pressure values from molecular line data towards Sim 129 and 130 are found to be 23×10^5cm^{-3} K and 21×10^5cm^{-3} K, respectively. The IBL pressure is ascertained to be comparable to the internal pressure in the nebulae which suggests that these nebulae are in a state of pressure balance.

4.5 Triggered Star Formation in Sim Nebulae

Recently Lim et al. (2018) reported evidence for feedback-driven star formation in NGC 1893 using high-resolution spectroscopy of stars and gas in the young open cluster NGC 1893. Their results suggest that newborn stars and the tadpole nebula Sim 130 are moving away from the central cluster containing O-type stars. They estimated a sequential star formation time scale of $\sim$1 Myr within a 9 pc distance. They asserted that $\sim$ 18 percent of the total population of stars are formed by feedback from massive stars. This finding suggests that this process might have helped in the formation of the OB association. The results presented by Lim et al. (2018) also support the self-regulating star formation model (Elmegreen & Lada 1977).

4.6 Kinematics of Sim Nebulae

Recently, Ortega et al. (2020) published the kinematics of these two nebulae Sim 129 and 130 utilizing multiple gas tracers such as ^{12}CO (J=3–2), HCO$^+$, C_2H, HNC and HCN J=4–3 transitions. They detected kinematic signatures of infalling gas in the ^{12}CO (J=3–2) and C_2H

J=4–3 spectra toward Sim 129. However, they noted that the possible star formation activity in Sim 130 has not started yet when they analyzed the HCN/HNC integrated ratio of approximately three. Our profile of ^{12}CO (J=1–0) gas from TRAO observations in this region mostly matches their higher profile from high transition CO gas. This suggests that the gas motion is almost intact and coherent in low and high density regimes. Ortega et al. also stated that Sim 129 may be in a much more evolved stage with star formation activity inside the head part of the globule. This finding was supported by their non-detection of optically thin tracers such as HCN and HNC in Sim 129. This could be due to radiation from the newly formed star(s) in Sim 129.

5 SUMMARY

The nebulous emission and structures in the NGC 1893 region are revealed using 1.4 GHz observations from NVSS archival data. Sim 129 and Sim 130 are nebulae that have undergone photoionization in the vicinity of five O type stars including HD 242935. The magnetic field lines towards the head of the nebulae seem to be intact towards both nebulae, resulting in a curved field orientation. This happens generally when the field lines are perpendicular to the ionizing photons. Some polarization vectors are found to follow the radio emission, suggesting magnetic fields are dragged away by ionizing radiation from the central O type star. The ^{12}CO (J=1–0) molecular line observations are used to measure the velocity dispersion required for estimating the magnetic field strength from the DCF relation. The plane of the sky magnetic field strength is ascertained to be $\sim 60\,\mu$G with uncertainty of 0.5 times the estimated strength towards the region covered with polarization observations. The IBL pressure is found to be comparable to the internal pressure in Sim nebulae, suggesting that the nebulae are in a state of photoionization induced pressure balance. Recently evidence of feedback triggered star formation was identified in NGC 1893, supporting the self-regulating star formation model.

Acknowledgements I thank the anonymous referee for a very constructive report. I also thank NSF funding (1715876) for partially supporting this research. I also acknowledge KASI postdoctoral funding while this project was in progress in 2017. I thank Dr. Chang Won Lee and Dr. Maheswar for discussion on this project.

References

Bailer-Jones, C. A. L., Rybizki, J., Fouesneau, M., et al. 2018, AJ, 156, 58
Bertoldi, F. 1989, ApJ, 346, 735
Chandrasekhar, S., & Fermi, E. 1953, ApJ, 118, 113
Crutcher, R. 2005, in The Magnetized Plasma in Galaxy Evolution, eds. K. T. Chyzy, K. Otmianowska-Mazur, M. Soida, & R.-J. Dettmar, 103
Davis, L. 1951, Physical Review, 81, 890
Elmegreen, B. G., & Lada, C. J. 1977, ApJ, 214, 725
Eswaraiah, C., Pandey, A. K., Maheswar, G., et al. 2011, MNRAS, 411, 1418
Franco, G. A. P., Alves, F. O., & Girart, J. M. 2010, ApJ, 723, 146
Henney, W. J., Arthur, S. J., de Colle, F., & Mellema, G. 2009, MNRAS, 398, 157
Jose, J., Pandey, A. K., Ojha, D. K., et al. 2008, MNRAS, 384, 1675
Killeen, N. E. B., Bicknell, G. V., & Ekers, R. D. 1986, ApJ, 302, 306
Lai, S.-P., Crutcher, R. M., Girart, J. M., & Rao, R. 2001, ApJ, 561, 864
Lefloch, B., & Lazareff, B. 1994, A&A, 289, 559
Lim, B., Sung, H., Bessell, M. S., et al. 2018, MNRAS, 477, 1993
Liu, T., Kim, K.-T., Juvela, M., et al. 2018, ApJS, 234, 28
Mackey, J., & Lim, A. J. 2011, MNRAS, 412, 2079
Maheswar, G., Sharma, S., Biman, J. M., et al. 2007, MNRAS, 379, 1237
Morgan, L. K., Thompson, M. A., Urquhart, J. S., et al. 2004, A&A, 426, 535
Negueruela, I., Marco, A., Israel, G. L., & Bernabeu, G. 2007, A&A, 471, 485
Ortega, M. E., Paron, S., Areal, M. B., & Rubio, M. 2020, A&A, 633, A27
Schmidt, G. D., Elston, R., & Lupie, O. L. 1992, AJ, 104, 1563
Serkowski, K. 1974, Polarization Techniques., Astrophysics, Part A: Optical and Infrared, 361
Sharma, S., Pandey, A. K., Ojha, D. K., et al. 2007, MNRAS, 380, 1141
Soam, A., Maheswar, G., Bhatt, H. C., et al. 2013, MNRAS, 432, 1502
Soam, A., Maheswar, G., Lee, C. W., et al. 2015, A&A, 573, A34
Soam, A., Maheswar, G., Lee, C. W., et al. 2018, MNRAS, 476, 4782
Sohn, B. W. 2011, Journal of Astronomy and Space Sciences, 28, 267
Sugitani, K., Fukui, Y., & Ogura, K. 1991, ApJS, 77, 59
Targon, C. G., Rodrigues, C. V., Cerqueira, A. H., & Hickel, G. R. 2011, ApJ, 743, 54
Thompson, M. A., Urquhart, J. S., & White, G. J. 2004, A&A, 415, 627
Wardle, J. F. C., & Kronberg, P. P. 1974, ApJ, 194, 249
Williams, R. J. R., Ward-Thompson, D., & Whitworth, A. P. 2001, MNRAS, 327, 788
Zealey, W. J., Ninkov, Z., Rice, E., et al. 1983, Astrophys. Lett., 23, 119